Impacts of ball-milling on ZSM-5 zeolite properties and its catalytic activity in the two-phase glycerol ketalization with acetone

Diego S.D. Lima, Iago Zapelini, Laura Silva, Svetlana Mintova, Leandro Martins

Impacts of ball-milling on ZSM-5 zeolite properties and its catalytic activity in the two-phase glycerol ketalization with acetone

Diego S. D. Lima[a], Laura L. Silva[a], Iago W. Zapelini[a,b], Svetlana Mintova[b], Leandro Martins[a*]

[a]Universidade Estadual Paulista - Unesp, Institute of Chemistry, R. Prof. Francisco Degni, 55, 14800-900, Araraquara-SP, Brazil.
[b]Normandie Université, ENSICAEN, UNICAEN, CNRS, Laboratoire Catalyse et Spectrochimie (LCS), 6 Bd Maréchal Juin, 14000, Caen, France.

*leandro.martins@unesp.br

Abstract

A series of acidic ZSM-5 zeolites were mechanically ball-milled for different periods and further applied as catalysts in the liquid-phase glycerol ketalization with acetone. Structural and textural characterizations showed that the samples had considerable crystallinity and micropore volume loss due to amorphization. On the other hand, due to a comminution effect, the external surface area increased and particle size reduced. TPD and FTIR analyses with probe molecules with different sizes, such as ammonia, pyridine (Py), and 2,6-di-tert-butylpyridine (DTBPy) chemisorbed on the catalyst acid sites, aided in quantifying the different levels of accessibility of chemicals. The treated materials lost acidity due to amorphization or blockage of pores, but the milling enabled higher accessibility of bulkier chemicals to acid sites, as revealed by the chemisorption of Py and DTBPy. A crucial balance of acidity and accessibility was tailored by milling time. The one-hour grounded zeolite had a glycerol conversion 35% greater than the pristine sample and 67% greater than the eight-hour milled sample. The results showed that ball milling is a tool to improve the catalytic activity of zeolites with bulky chemicals by fine-tuning the milling time.

keywords: mesoporous zeolites, milling time, accessibility, chemisorbed pyridines

Graphical abstract

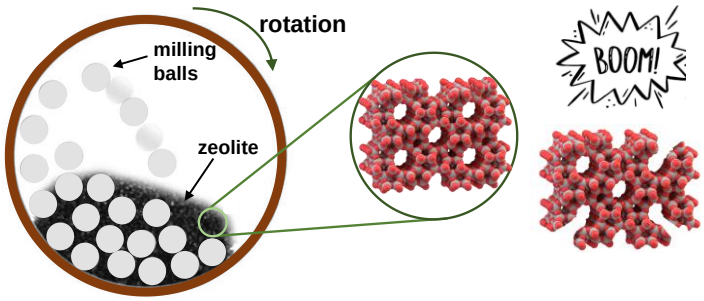

Highlights

- ✓ The mechanical treatment led to the disaggregation of particles and the breaking of Si-O-T bonds.
- ✓ The specific external area experiences a maximum, as reaggregation occurs over long periods.
- ✓ Increased accessibility in short ball-milling periods is beneficial for catalytic application.
- ✓ For two-phase reactions in which the hydrophobicity of the catalyst is important, excessive -T-OH defects impair the contact between phases.

1. Introduction

Zeolites are fundamental in biomass transformations, especially in up-grading bioderived platform molecules.[1] However, some challenges must be overcome for an extensive application in a biomass context. One of the highest obstacles is the intrinsic microporosity of these solids, which hampers the internal diffusion of bulky bioderived compounds.[2]

Several studies have shown that bottom-up and top-down processes are valuable alternatives for creating a secondary level of porosity (meso- or macropore) in zeolites to solve the microporosity issue.[2,3] From a bottom-up perspective, Kelkar et al.[4] enabled a higher selectivity for aromatics in biomass pyrolysis, creating mesopore regions using structure-direct agents in the synthesis. While in a top-down perspective, Arias et al.[5] exfoliated sheets of MWW zeolite to improve the selectivity and yield in ketalization of glycerol with 5-hydroxymethylfurfural. Although the current proposals are promising for applying zeolitic materials in biomass processing, the high cost and multi-step synthesis methods are undesirable inconveniences.[2]

In this context, ball-milling is a low-cost, practical, and efficient method for improving zeolite reactivity by mechanical activation.[6-8] Its action can rapidly induce important structural and morphological changes using minimal amounts or no solvent.[6] These modifications are beneficial for the application of zeolites in heterogeneous catalysis.

Considering the catalysis perspective, the main desirable modification is the comminution of the particles by breaking zeolite crystals into small crystalline pieces. That effect leads to a higher exposition of acid sites, improving the activity of the catalyst in reaction with bulky molecules. Zielinski et al.[9] increased the catalytic cracking of bulky hydrocarbons in zeolites due to improved accessibility of the acid sites after milling. Besides, Wakihara et al.[10] noticed that the size diminishment of the particles enabled higher resistance to deactivation by coke.

On the other hand, undesirable modifications in zeolites may arise after milling, such as amorphization and aggregation of particles, which are harmful to catalysis. Distinguishing the benefit from the damages these modifications may cause to the crystals is challenging because they depend on the time and energy of the mechanical treatment. Additionally, the zeolite framework, Si/Al ratio, and the presence or absence of water vapor may also influence.[6]

Although mechanochemistry has gained prominence in the zeolite field,[7] milling studies focus on applying the modified catalysts to hydrocarbon cracking reactions.[9-11] Investigating the use of mechano-treated zeolites in liquid-phase reactions and biomass valorization can enlarge the possibilities of mechanochemistry. Therefore,

herein, we investigated the structural and textural characteristics of ZSM-5 zeolites milled at different times and their application in the glycerol ketalization with acetone.

2. Experimental

2.1. Ball-milling of the catalysts

ZSM-5 zeolite of Si/Al ratio 25 and in the ammonium form was supplied by Zeolyst (CBV5524G). For the ball-milling, 1.8 g of the zeolite and ten alumina balls 20 mm in diameter were added to a cylindrical jar of 65 mm in diameter and 300 mL of volume. The system was then coupled to the ball-mill equipment and subjected to a transversal rotation at 400 rpm. The mechanical treatment varied between 0.5, 1, 2, 4, and 8 h.

2.2. Characterization

X-ray diffraction measurements of the powdered samples were performed in a Rigaku Model SmartLab, using Cu Kα radiation (40 kV, 15 mA) and 2θ acquisition range from 5 to 40° with a step size of 0.02° and goniometer speed of $2°.min^{-1}$.

Scanning electron microscopy (SEM) was used to examine the effects of ball milling on the samples' particle sizes and morphologies. Before, 50 mg of samples were dispersed in isopropyl alcohol and sonicated for 30 min. Droplets were dispersed onto an aluminum sample holder and analyzed in an FEI Magellan 400L microscope operated at 25 kV. The average particle size was determined considering the average size of at least 200 particles.

Nitrogen physisorption measurements at 77 K were performed in an ASAP 2010 Micromeritics instrument to determine the textural properties of the zeolites. Previously, 200 mg of each sample was degassed under vacuum for 12 h at 250 °C.

Solid-state ^{27}Al MAS NMR was performed to investigate the aluminum species present in the zeolites. The powdered samples were packed into 4 mm zirconia rotors. All the experiments were performed at 25 °C with a 10 kHz spinning rate. The spectra were recorded in a Bruker Avance III 400 MHz spectrometer equipped with a standard Bruker 4 mm magic-angle spinning (MAS) probe, operating at 104.21 MHz for ^{27}Al.

The acidity of the zeolites was determined by the desorption of ammonia at a programmed temperature (NH_3-TPD). Previously, 200 mg of the zeolite in the H^+-form was pre-treated at 400 °C, under a He flow of 60 $mL.min^{-1}$ for 1 h, then cooled to 100 °C. Then, a flow containing 1 % of NH_3 in He for 1 h was used to guarantee the whole adsorption of NH_3. Further, the samples were subjected to a flow of pure helium for 2 h at 100 °C to remove the adsorbed ammonia. Finally, the ammonia molecules adsorbed on the acid sites were desorbed by heating the samples to 500 °C at a ramp of 10 $°C.min^{-1}$ and monitored by a Pfeiffer Vacuum mass spectrometer connected to the reactor outlet.

Further acidity characterization of the samples by pyridine (Py) and 2,6-di-tert-butylpyridine (DTBPy) chemisorption was monitored in situ by Fourier-Transform Infrared (FTIR) spectra recorded with a Thermo Scientific Nicolet iS50 FTIR spectrometer equipped with an MCT detector, at a spectral resolution of 4 cm^{-1}. Measurements were performed using self-supported disks of about 20 mg. The samples were previously degassed at 450 °C for 4 h under a 10^{-5} Torr vacuum. The spectra of degassed samples were collected at room temperature, used for hydroxyl characterization, and further subtracted after adsorption of the probe molecules. Probe molecules were delivered in the cell at room temperature (1 Torr for Py and 0.2 Torr for DTBPy)[12] followed by a treatment at 150 °C for 30 min for diffusion. The chemisorbed Py or DTBPy spectra were acquired after the desorption step at 150 °C for 15 min under vacuum. The total concentration of the Brønsted (BAS) and Lewis (LAS) acid sites was calculated via integration of the peaks at approximately 1545 and 1454 cm^{-1}, raised in Py chemisorption experiments, with extinction coefficients of 1.72 for LAS and 1.30 $cm.\mu mol^{-1}$ for BAS quantification by the Beer-Lambert equation.[13] The peak raised at around 1540 cm^{-1} in the DTBPy chemisorption experiment was used for external BAS (EBAS) quantification using the extinction coefficient of 1.30 $cm.\mu mol^{-1}$.[14]

The hydrophobicity-hydrophilicity of the samples was measured by glycerol contact angle using a DataPhysics OCA equipment coupled with a CCD camera. The contact angle between the sample wafer (previously dried under vacuum overnight) and a 20 µL glycerol droplet was calculated based on the mean value of 3 measurements.

2.3. Catalytic test

The condensation reaction of glycerol with acetone (Equation 1) was carried out in a 2 mL batch microreactor. In a typical experiment, 200 mg of glycerol and 2.37 g of acetone (glycerol/acetone molar ratio of 1:6) were added to the reactor containing 20 mg of catalyst. The mixture was magnetically stirred from 5 to 80 min at 40 °C. The products were analyzed in a gas chromatograph (GC-2014, Shimadzu) equipped with a capillary column (Rtx-1, 30 m, 0.32 mm internal diameter, and 1 µm film thickness) and an FID detector. Before each injection, *circa* 0.09 g of n-butanol was added as an internal standard to carry out a quantitative mass balance of glycerol, acetone, and condensation products, solketal ((2,2-dimethyl-1, 3-dioxolan-4-yl) methanol) or dioxane (2,2-dimethyl-dioxan-5-ol). The retention times of all products were obtained by injecting standards.

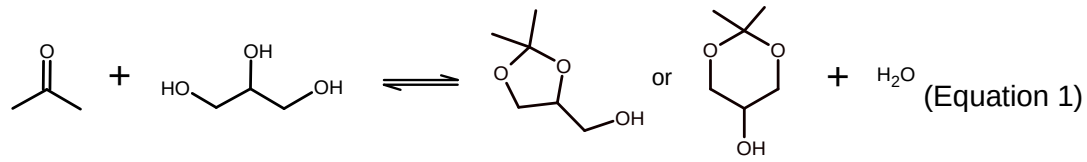

Acetone Glycerol Solketal Dioxane (Equation 1)

The initial turnover frequency, TOF_0, was calculated based on the glycerol conversion at time zero, allowing a more reliable comparison of the performance of different catalysts. The kinetic data were adjusted by Equation 2, where X (%) is the glycerol conversion and *t* (in min) is the time. Parameters *a* and *b* were obtained from the least squares fitting, considering five conversion measures at different times (5, 10, 20, 40, and 80 min). Finally, the TOF_0 was calculated according to Equation 3, where N_0 corresponds to moles of glycerol added to the reactor and [acid sites] the moles of sites determined from Py-FTIR measurements.

$$X(\%) = \frac{a\,.\,t}{b+t} \qquad \text{(Equation 2)}$$

$$TOF_0 = \frac{N_0\left(\frac{dX(\%)}{dt}\right)_{t=0}}{[acid\ sites].100} \qquad \text{(Equation 3)}$$

3. Results and Discussion

3.1. Characterization of the catalysts

Figure 1a shows the diffractograms of the ball-milled samples, together with the Rietveld refinement that revealed considerable variations in unit cell volumes and crystallite sizes. Additionally, all the lattice parameters (a, b, and c in Table 1S) had a general increasing tendency and decrease of β angle, which promoted cell volume expansion (Fig. 1b). The structural modifications and distortions indicate mechanical activation.[13] The balls' kinetic energy also promoted bond ruptures, creating defects.[15,16] The accumulation of defects implicates the formation of crystal cracks and further fractures.[17] Given this, the crystallite size diminished, reducing the size from 144.2 to 98.8 nm in 8 h of milling.

Concerning the XRD pattern, all the samples presented the characteristic MFI diffraction peaks in the 7-9° and 22-25º ranges. However, the gradual decrease of peak intensity compared to the untreated sample indicates a loss of crystallinity.[10] The characteristic peak area in the 22 to 25° range was used to calculate the degree of relative crystallinity (Fig. 1c),[18] accompanied by quantitative textural information. The curves in Fig. 1c had the same tendency for micropore volume and relative crystallinity, which initially decreased fast and slowly after 4 h. It suggests an amorphization process due to the mechanical treatment.[8] The process is related to the extensive breakage of external Si-O-T (T = Si or Al) bonds in zeolite structure and the destruction of part of the pores and consequent blockage.[9,10,17,19] The degree of destruction depends on the milling energy.[20] Considering that after 8 h of milling, there is a relative

stabilization of textural and crystallinity parameters, a higher amorphization degree would be reached through higher milling frequencies.

On the other hand, the external surface area behavior diverges from the profile of the micropore volume and relative crystallinity curves. At the beginning of the mechanical treatment, the external surface area increased, reaching a maximum at 1 h, and quickly diminishing. The same behavior occurred in similar studies.[9,21,22] The initial stage resembles the dispersion phase, in which fractures in the crystals[11] or the separation of crystalline agglomerates promote the increase in the external area.[17] Otherwise, an opposite effect is the aggregation, which occurs after longer milling times. In that step, the crystal size still tends to decrease while the external area diminishes because of the compression of the small fragments and fractured crystals between the balls and the vessel's walls,[23] forming bigger agglomerates with lower external area.[17,22] The complete nitrogen adsorption isotherms together with the BJH pore size distribution method, in Fig. 1S in supplementary material, show that in addition to these textural changes, there is the systematic emergence of pores upon the mechanical treatment in the meso- and macropore regions. The macropores might originate from a disaggregation process, and the mesopores from a Si-O-T bond-breaking process.

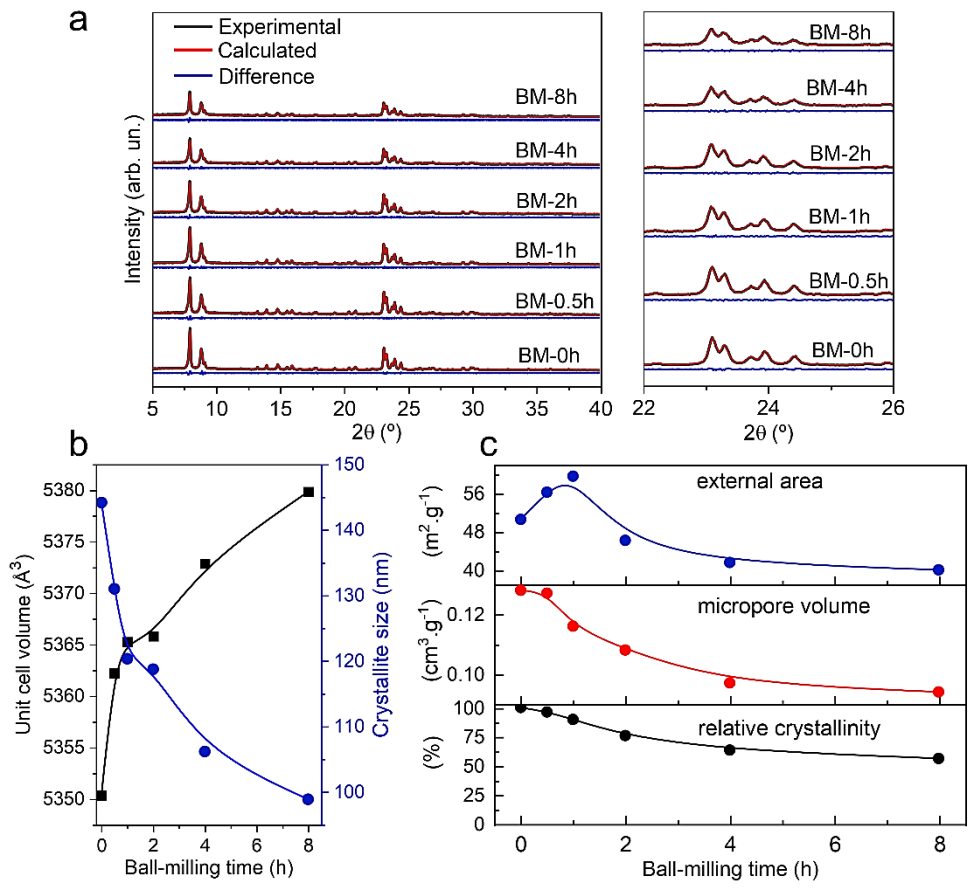

Fig. 1 - Structural and textural properties of ball-milled ZSM-5 samples: (a) X-ray diffraction patterns, (b) unit cell volume, and (c) crystallite sizes as a function of milling time, (d) external area, micropore volume, and relative crystallinity as a function of milling time.

The pristine sample (BM-0 h) and those submitted to 1 and 8 h of milling stand as key samples to follow the mechanical activation as they have varied properties. Thus, further analyses were carried out for the three samples to comprehend their properties. Fig. 2 presents the scanning electron microscopy (SEM) images of samples at selected milling times. The BM-0h particles do not show a regular and homogeneous shape due to many small agglomerates of crystals with edges and sharp shapes. Those particles ranged between 0.1 and 0.7 nm in size, with an average of 0.28 nm. The BM-1h material had a highly similar morphology to the pristine sample. However, smaller aggregates were noticed because of the comminution, causing the separation and breakage of bigger particles in the dispersion step.[21,22] That effect diminished the particles' average size to 0.24 nm and reduced the size dispersion between 0.1 and 0.5 nm, resulting in a less broad distribution.

In contrast, the BM-8h sample had expressive changes in morphology, evidenced by the formation of small particles with spherical shapes. At the same time, a new agglomeration pattern is noticed, composed of many small spherical particles building large agglomerates that arose in the aggregation step.[21,22] The presence of small particles led to a drop in average particle size to 0.17 nm. The high agglomeration level created large aggregates that did not contribute at all to the distribution size. Therefore, the decrease in the external areas is intrinsically associated with forming agglomerates.

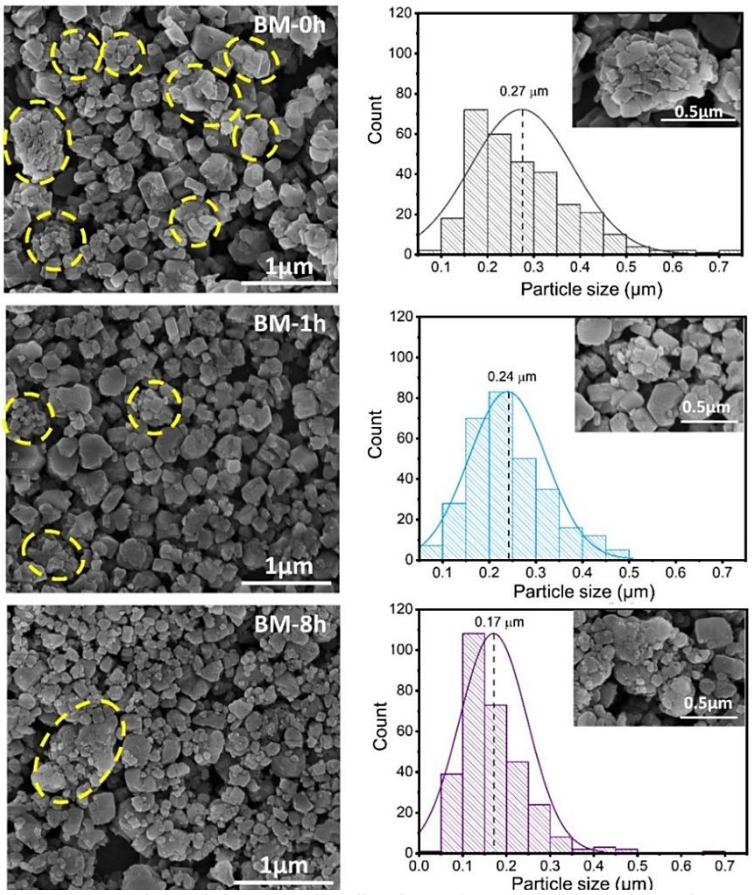

Fig. 2 - SEM images and particle size distribution of BM-0h, BM-1h and BM-8h samples.

In NMR ^{27}Al spectra (Fig. 3a), two significant peaks are observed: the one at the chemical shift around 55 ppm and the second around 0 ppm. Both are associated with the coordination of aluminum. The first resembles the resonance of tetrahedrally coordinated aluminum atoms (AlO_4) in a zeolite framework. The second relates to hexacoordinated aluminum atoms (AlO_6), which can be associated with extra framework or partially bonded species to the zeolite framework.[24,25] Those species include unspecified aluminum species in oxides and hydroxide forms. Independently of their specific nature, the relative quantity increased for the mechanically treated samples due to the breakage of Si-O-Al bonds and the removal of Al from the zeolite structure, leading to a higher number of hexacoordinated aluminum species.

The IR spectra in the OH region shown in Fig. 3b confirm the structural rupture of the zeolite. The strong band at 3612 cm^{-1} resembles the vibration of bridged OH bonded to Si and Al atoms.[26,27] The variation in intensity between BM-0h and BM-1h samples was unnoticeable in that wavenumber. Otherwise, for BM-8h, a considerable decrease was observed, suggesting a loss of acid sites. Additionally, the wavenumber ranging from 3670 to 3650 cm^{-1} is related to OH stretching linked to the extraframework aluminum.[18] BM-1h and BM-8h had an increase in that region compared to BM-0h, which is related to the superior amount of AlO_6 (following the ^{27}Al-NMR signal). Finally,

the large band with a central peak at 3744 cm^{-1} is related to the OH stretching of isolated silanols. In contrast, for lower frequencies, there are multiple contributions of internal silanols and interacting silanols,[28] as was evident for the BM-8h sample, subjected to long mechanical treatment that created many defects due to breakage of bonds. Interestingly, the increment in silanols concentration was more pronounced in vicinal silanols than in isolated ones. It is explained by the aggregation, wherein the larger proximity between small crystals allows enhanced interactions between surface silanols.

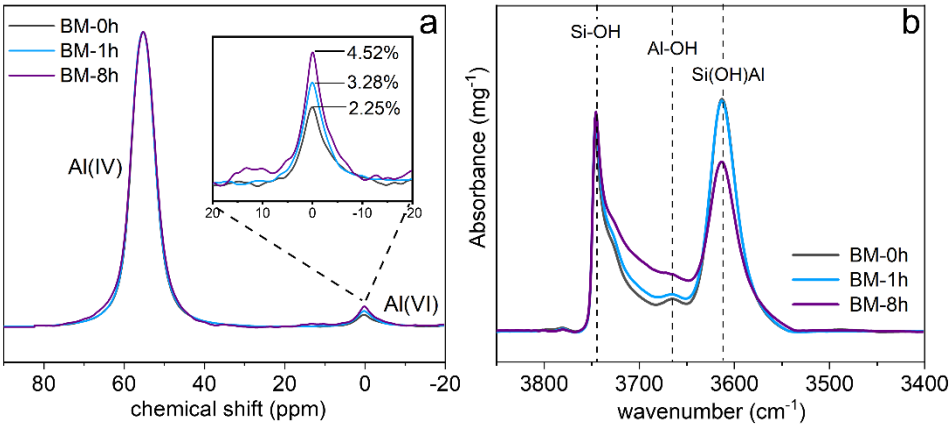

Fig. 3 - (a) ^{27}Al NMR and (b) IR spectra in the hydroxyl region of BM-0h, BM-1h, and BM-8h samples.

TPD and FTIR were used to quantify the number of acid sites and their accessibility with the probe molecules of different sizes: ammonia ($\sigma_{Ammonia}$ = 0.38 nm), pyridine (σ_{Py} = 0.54 nm), and 2,6-ditertbutyl-pyridine (σ_{dTBPy} = 1.05 nm). The ZSM-5 zeolite presents pores with openings of 0.53 x 0.56 nm and 0.51 x 0.55 nm. Thus, the three probe molecules used herein can reach the acid sites differently. The acidity results perceived by the three molecules are shown in Fig. 4 (Fig. 2S and Table 2S). Firstly, the ammonia molecules can easily access the zeolite pores, which justifies the higher quantification of acid sites than pyridine. Regarding the use of ammonia, BM-1h had a higher number of total acid sites than BM-0h, which is associated with a slightly higher quantity of accessible acid sites. Otherwise, after 8 h of milling, the zeolite significantly lost acid sites due to amorphization[29,30] and/or blockage of the pores. Regarding FTIR-Py, the pyridine has a kinetic diameter close to the pore opening of the zeolite. However, due to the similarity of diameters, pyridine molecules diffuse mostly in a configurational profile, presenting diffusional limitations, which prevents them from accessing a few acid sites.[31] The BM-1h presented the highest number of acid sites probed by pyridine because it has more accessible sites for molecules with similar dimensions to pyridine. The comminution effect during the milling justifies the increase

in accessibility. Following the structural and textural modifications of the BM-8h sample, the chemisorption of ammonia also perceived a high loss of acidity. The pyridine chemisorption can differentiate Brønsted (BAS) and Lewis acid sites (LAS), therefore, the specific increase in Py-LAS in Table 1 is associated with an increase in AlO_6 species.[25,32] Regarding FTIR-DTBPy, the BM-8h presented the highest quantity. The DTBPy molecule is too large to access the zeolite's pores, thus adsorbing only onto external sites. The sample milled for 8 h lost a considerable part of the acid sites; however, the remaining acid sites were external and more accessible due to the high level of crystal breakage.

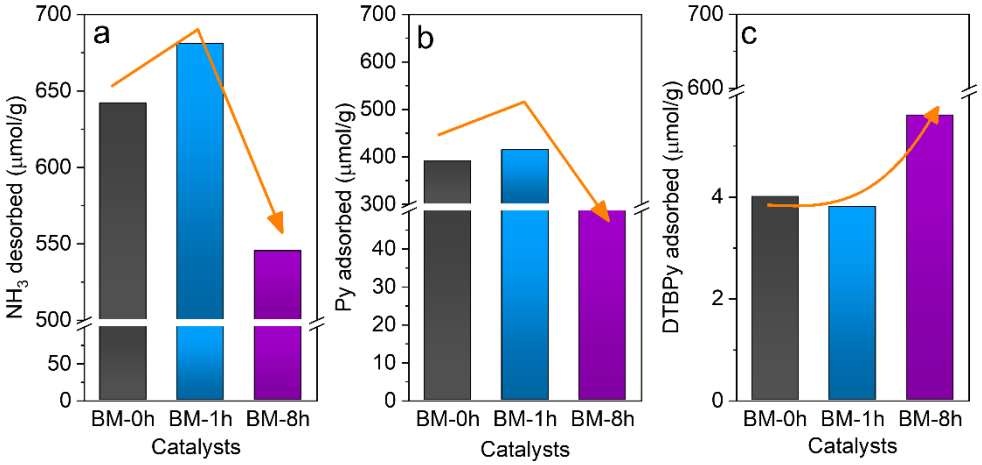

Fig. 4 - Acidity measurements of BM-0h, BM-1h, and BM-8h samples by (a) TPD-NH_3, (b) FTIR-Py and (c) FTIR-DTBPy.

3.2. Catalytic application

Due to the polarity of glycerol, its solubilization in acetone is low, limited to approximately 5% wt.,[33] which impacts the rate of the ketalization reaction. In this situation of low solubility, the reaction takes place in two phases. In a solvent-free medium, the acetal formation only occurs in the phase boundary, where glycerol-acetone interactions can exist freely.[34] Therefore, mixing the reaction media is fundamental for the glycerol dispersion into droplets, maximizing the phase-boundary region.[35] In this context, the catalyst may have an additional functionality by acting as an intermediate in regulating the contact of both phases. In previous studies,[36,37] we have learned that the adjustment of the hydrophobic-hydrophilic character of the catalyst plays an important role in maximizing the contact of phases.

Moreover, the solketal, the main reaction product, can act as a solvent during the reaction, improving glycerol miscibility and turning the system monophasic. According to Rahaman et al.,[38] after 25% of solketal formation, the system tends to become one-phase. However, turning the reaction media into one phase is just a portion of the solution because the diffusion of chemicals into the pores of the zeolites is an evident obstacle to the reaction.

In light of the properties of the glycerol ketalization reaction, the catalytic activity of the zeolites was assessed only up to 10 min of reaction when the solketal formation was below 25%, and the two-phase system was present. Therefore, we were able to assess both the capability of the catalyst to mix the reaction mixture and the improved diffusion of chemicals into its pores. The catalytic results are exposed in Fig. 5a. The glycerol conversion tended to increase for milled catalysts until 1 h of milling and decreased further. It shows that the catalytic activity can be adjusted by managing the milling time.

Previous studies pointed out the mechanical activation process has different stages of structural and energy changes in the materials that impact its reactivity.[15,16] In the initial stages, the accumulation of energy delivered to the solid creates defects and cracks that diminish particle size and increase the surface area. Those modifications generally lead to reactivity increment.[16] Otherwise, in the further stage, the excess of lattice modification leads to some amorphization of the material, forming samples with large debris associated with reduced reactivity. Although these stages include several complex sub-steps and their boundary are not sharply defined, it is possible to state that the glycerol conversion profile indicates the regions of reactivity of the catalyst as a function of the extension of milling treatment.

The glycerol and acetone molecules have a kinetic diameter comparable to the size of the ZSM-5 pores (σ_{gly} = 0.54 nm; σ_{ace} = 0.51 nm), while solketal and dioxane are larger than the pore opening, 0.61 nm. Therefore, the molecules have low diffusion capacity inside the pores, which is reasonable to assume that the reaction occurs preferably on the external surface.[37] As observed by FTIR-Py analyses, pyridine molecules also cannot access all acid sites due to steric hindrance. In addition, since its dimension is similar to glycerol and acetone molecules, we can assume that Py adsorption is a descriptor of the accessibility of chemicals to the acid sites. Thus, the catalyst performance in the reaction follows the same order as the acidity revealed by the FTIR-Py analysis: BM-1h > BM-0h > BM-8h.

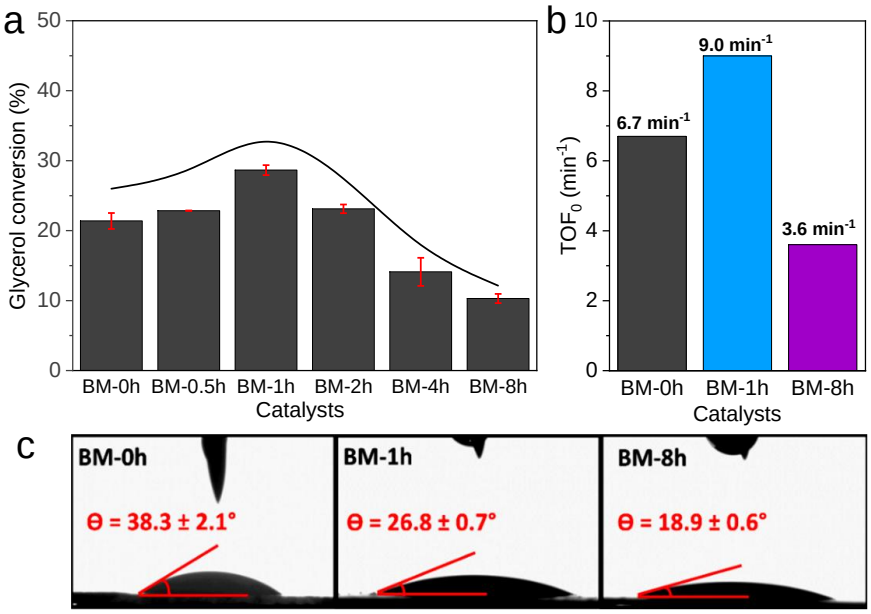

Fig. 5 - (a) Glycerol conversion for 10 min of reaction on ball-milled samples, (b) TOF_0 and (c) glycerol contact angle images for BM-0h, BM-1h, and BM-8h samples.

Zielinski et al.[9] have reached similar catalytic results in converting hydrocarbons with different kinetic diameters. Similarly, as studied herein, the catalysts with low milling periods led to higher conversions than longer periods as a function of mechanical activation. Furthermore, the authors noticed that the reactions with bulkier chemicals benefited the most since the molecules accessed more acid sites in milled materials than in pristine samples.

The kinetics of the reaction catalyzed by BM-0h, BM-1h, and BM-8h were monitored until 80 min (Fig. 3S), and their performances were analyzed in terms of TOF_0. The results presented the same trend as conversion: BM-1h > BM-0h > BM-8h. Interestingly, the BM-8h had the lowest TOF_0, although it had the most accessible sites for bulky molecules, as seen by FTIR-DTBPy results. That finding shows that although the molecules should have lower diffusional issues, the ketalization reaction was impaired. In this regard, BM-1h presented the optimal tailoring in accessibility, wherein the creation of more accessible sites preserved the majority of microporosity.

The low activity of the BM-8h can also be explained by the contact angle of glycerol on the zeolites measurements (Fig. 5c). A diminished contact angle is noticed, resulting from a stronger interaction of the catalyst surface with glycerol. That tendency suggests a high hydrophilic surface of the structure that can result from increased hydroxyl groups (Si-OH and Al-OH) in the structure, assigned as defects. Since BM-8h presented the highest interaction with glycerol, it can lessen its conversion since the catalyst tends to be placed in the glycerol phase at the bottom of the reactor, denser

than acetone. In contrast, the BM-1h catalyst with moderate interaction tends to be placed in the interphase region, where the reaction occurs more rapidly.

4. Conclusions

Herein, we have ball-milled ZSM-5 zeolites at different times to investigate the changes in their structural and textural properties. The micropore volume and crystallinity decreased for all periods due to the amorphization process. Otherwise, the external area increased up to 1 h of milling due to the breakage of crystals and disaggregation of larger particles. Furthermore, in 1 h of milling, higher accessibility for acid sites for molecules with similar dimensions to pyridine was reached, as noticed by FTIR-Py. The samples were applied in glycerol ketalization to evaluate their catalytic activity. A strong dependence was observed between milling time and glycerol conversion since the structural changes impact the number and accessibility of acid sites. Given this, the glycerol conversion tendency obeyed the FTIR-Py results: BM-1h > BM-0h > BM-8h. That similarity occurred because glycerol and acetone present similar dimensions to pyridine, thus being a suitable probe molecule to track the accessibility to the acid sites.

Ball-milling can be a practical and low-cost alternative for zeolite modification in biomass valorization. It improves the accessibility of acid sites, allowing bulky molecules to react more easily. Considering the balance of accessibility and the number of acid sites, the milling time must be tailored to reach higher accessibility and lower loss of acid sites.

Acknowledgments

The authors are grateful for the financial support granted by the São Paulo Research Foundation - FAPESP grants #2018/01258-5, #2019/12486-1, #2021/08326-9 and #2022/01789-6. We also acknowledge the GFQM/UNESP for the contact angle measurements and N_2 physisorption and the LCE/UFSCar for the scanning electron microscopy images.

5. References

1 T. Ennaert, J. Van Aelst, J. Dijkmans, R. De Clercq, W. Schutyser, M. Dusselier, D. Verboekend, B. F. Sels, Chem. Soc. Rev. 45 (2016) 584-611.
2 S. Mardiana, N. J. Azhari, T. Ilmi, G. T. M. Kadja, Fuel 309 (2022) 122119.
3 J. Přech, P. Pizarro, D. P. Serrano, J. Áejka, Chem. Soc. Rev. 47 (2018) 8263-8306.
4 S. Kelkar, C. M. Saffron, Z. Li, S. S. Kim, T. J. Pinnavaia, D. J. Miller, R. Kriegel, Green Chem. 16 (2014) 803-812.
5 K. S. Arias, M. J. Climent, A. Corma, S. Iborra, Energy Environ. Sci. 8 (2015) 317-331.
6 G. Majano, L. Borchardt, S. Mitchell, V. Valtchev, J. Pérez-Ramírez, Microporous Mesoporous Mater. 194 (2014) 106-114.
7 D. N. Rainer, R. E. Morris, Dalton Trans. 50 (2021) 8995-9009.

8 S. Koç, N. Toplan, K. Yildiz, H. Ö. Toplan, J. Therm. Anal. Calorim. 103 (2011) 791-796.
9 P. A. Zielinski, A. Vanneste, D. B. Akolekar, S. Kaliaguine, Microporous Mater. 5 (1995) 123-133.
10 T. Wakihara, A. Ihara, S. Inagaki, J. Tatami, K. Sato, K. Komeya, T. Meguro, Y. Kubota, A. Nakahira, Cryst. Growth Des. 11 (2011) 5153-5158.
11 L. L. Silva, M. J. Stellato, M. V. Rodrigues, B. J. Hare, J. C. Kenvin, A. S. Bommarius, L. Martins, C. Sievers, J. Catal. 411 (2022) 187-192.
12 L. Lakiss, A. Vicente, J.-P. Gilson, V. Valtchev, S. Mintova, A. Vimont, R. Bedard, S. Abdo, J. Bricker, *ChemPhysChem 21* (2020) 1873-1881.
13 J. Datka, A. M. Turek, J. M. Jehng, I. E. Wachs, J. Catal. 135 (1992) 186-199.
14 N. D. Shcherban, R. Y. Barakov, P. Maki-Arvela, S. A. Sergiienko, I. Bezverkhyy, K. Eranen, D. Y. Murzin, Appl. Catal., A 560 (2018) 236-247.
15 M. M. Ristic, S. Dj. Milosevic, Mechanical Activation of Inorganic Materials, Serbian Academy of Science and Arts, 1998.
16 P. Baláž, M. Achimovicová, M. Baláž, P. Billik, C. Z. Zara, J. M. Criado, F. Delogu, E. Dutková, E. Gaffet, F. J. Gotor, R. Kumar, I. Mitov, T. Rojac, M. Senna, A. Streletskii, W. C. Krystyna, Chem. Soc. Rev. 42 (2013) 7571-7637.
17 A. S. Kharitonov, V. B. Fenelonov, T. P. Voskresenskaya, N. A. Rudina, V. V. Molchanov, L. M. Plyasova, G. I. Panov, Zeolites 15 (1995) 253-258.
18 Y. Sun, T. Ma, S. Cao, J. Wang, X. Meng, Y. Gong, Z. Zhang, A. Ma, P. Liu, Microporous Mesoporous Mater. 326 (2021) 111360.
19 T. Tunç, A. Ş. Demirkiran, Powder Technol. 260 (2014) 7-14.
20 V. Sydorchuk, V. Vasylechko, O. Khyzhun, G. Gryshchouk, S. Khalameida, L. Vasylechko, Appl. Catal., A 610 (2021) 117930.
21 K. Akçay, A. Sirkecioğlu, M. Tatlier, Ö. T. Savaşçi, A. Erdem-Şenatalar, Powder Technol. 142 (2004) 121-128.
22 C. Kosanovic, J. Bronic, A. Cizmek, B. Subotic, I. Smit, M. Stubicar, A. Tonejc, Zeolites, 15 (1995) 247-251.
23 C. Kosanovic, A. Cizmek, B. Subotic, I. Smit, M. Stubicar, A. Tonejc, Zeolites 15 (1995) 51-57.
24 L. G. Possato, R. N. Diniz, T. Garetto, S. H. Pulcinelli, C. V. Santilli, L. Martins, J. Catal. 300 (2013) 102-112.
25 M. Ravi, V. L. Sushkevich, J. A. van Bokhoven, Nat. Mater. 19 (2020) 1047-1056.
26 R. Borade, A. Sayari, A. Adnot, S. Kaliaguine, J. Phys. Chem. 94 (1990) 5989-5994.
27 M. Trombetta, T. Armaroli, A. Gutierrez-Alejandre, J. R. Solis, G. Busca, Appl. Catal., A 192 (2000) 125-136.
28 P. Ayrault, J. Datka, S. Laforge, D. Martin, M. Guisnet, J. Phys. Chem. B, 108 (2004) 13755-13763.
29 A. Auroux, M. Huang, S. Kaliaguine, Langmuir 12 (1996) 4803-4807.
30 M. Huang, S. Kaliaguine, A. Auroux, J. Phys. Chem., 99 (1995) 9952-9959.
31 L. L. Silva, D. Cardoso, C. Sievers, L. Martins, J. Phys. Chem. C 124 (2020) 2439-2449.
32 G. Busca, Microporous Mesoporous Mater. 254 (2017) 3-16.
33 M. N. Moreira, R. P. V. Faria, A. M. Ribeiro, A. E. Rodrigues, Ind. Eng. Chem. Res. 58 (2019) 17746-17759.
34 V. Calvino-Casilda, K. Stawicka, M. Trejda, M. Ziolek, M. A. Bañares, J. Phys. Chem. C 118 (2014) 10780-10791.
35 S. D. Naik, L. K. Doraiswamy, AIChE J. 44 (1998) 612-646.
36 D. S. D. Lima, L. L. Silva, I. W. Zapelini, S. Mintova, L. Martins, Inorg. Chem. Front. 10 (2023) 5649-5661.
37 G. L. Catuzo, C. V. Santilli, L. Martins, Catal. Today 381 (2021) 215-223.

38 M. S. Rahaman, T. K. Phung, M. A. Hossain, E. Chowdhury, S. Tulaphol, S. B. Lalvani, M. O'Toole, G. A. Willing, J. B. Jasinski, M. Crocker, N. Sathitsuksanoh, Appl. Catal., A 592 (2020) 117369.

Suplementary material

Impacts of ball-milling on ZSM-5 zeolite properties and its catalytic activity in the two-phase glycerol ketalization with acetone

Diego S. D. Lima[a], Laura L. Silva[a], Iago W. Zapelini[a,b], Svetlana Mintova[b], Leandro Martins[a]

[a]Universidade Estadual Paulista - Unesp, Institute of Chemistry, R. Prof. Francisco Degni, 55, 14800-900, Araraquara-SP, Brazil.
[b]Normandie Université, ENSICAEN, UNICAEN, CNRS, Laboratoire Catalyse et Spectrochimie (LCS), 6 Bd Maréchal Juin, 14000, Caen, France.

Table 1S - Unit cell parameters of the ZSM-5 zeolite ball-milled at different times.

Cell parameters	Milling time (h)					
	0	0.5	1	2	4	8
a (Å)	19.872(9)	19.909(2)	19.912(3)	19.909(2)	19.914(1)	19.922(3)
b (Å)	20.101(4)	20.096(1)	20.102(4)	20.102(0)	20.112(6)	20.120(9)
c (Å)	13.394(0)	13.402(4)	13.403(7)	13.407(4)	13.414(8)	13.421(0)
β (º)	90.516(3)	90.177(0)	90.162(9)	90.186(6)	90.231(8)	90.204(3)

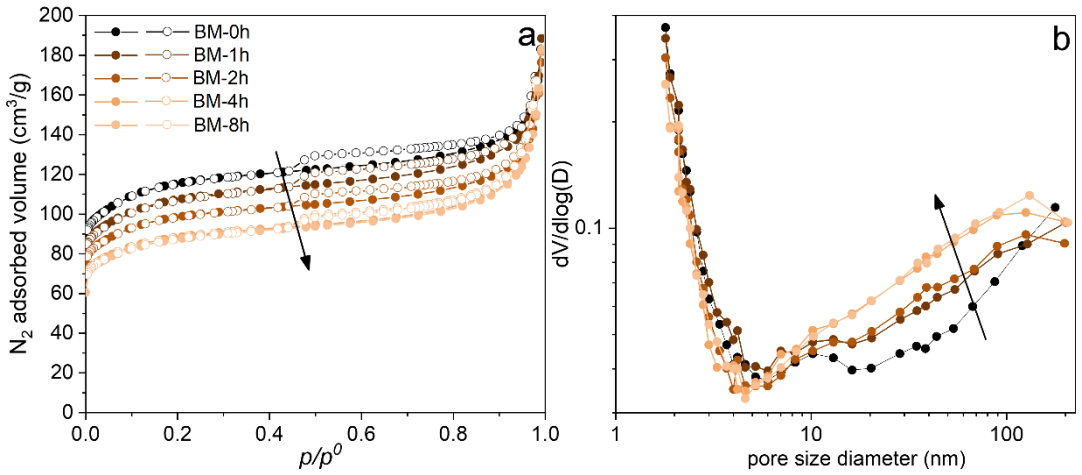

Fig. 1S - Physisorption measurements of ball-milled ZSM-5 zeolites: (a) nitrogen adsorption isotherms and (b) BJH method giving the pore size distribution in the meso and macropore region.

Table 2S - Acidity measurements of BM-0h, BM-1h, and BM-8h samples.

Catalysts	TPD-NH_3 (µmol $NH_3 \cdot g^{-1}$)			FTIR-Py (µmol·g^{-1}) - 150ºC			FTIR-DTBPy (µmol·g^{-1}) - 150ºC
	LT[1]	HT[2]	Total	BAS	LAS	Total	EBAS
BM-0h	239	403	642	332	58	390	4
BM-1h	286	395	681	343	71	414	3.8
BM-8h	205	340	545	221	77	298	5.6

1. LT - low temperature (NH_3 desorbed between 170-190 ºC), 2. HT - high temperature (NH_3 desorbed between 290-500 ºC).

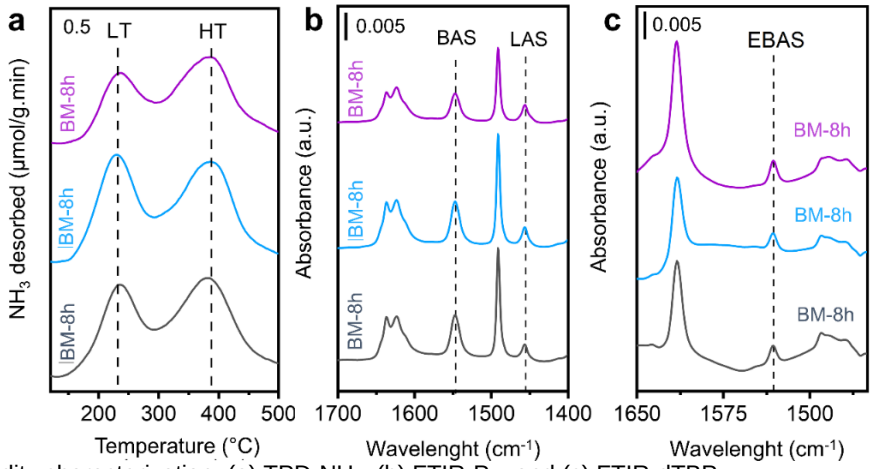

Fig. 2S - Acidity characterization: (a) TPD-NH_3, (b) FTIR-Py, and (c) FTIR-dTBPy.

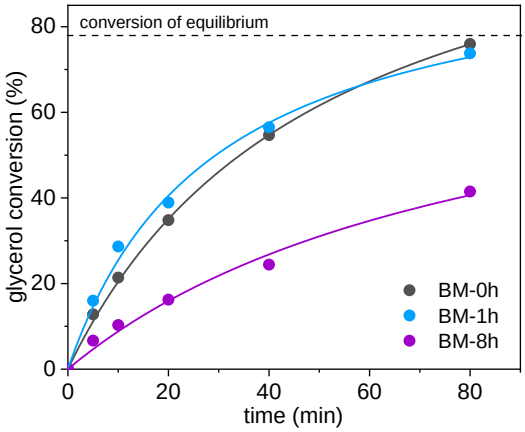

Fig. 3S - Glycerol conversion at different times using ball-milled ZSM-5 catalysts.